MODIFICATION OF BUOYANCY-DRIVEN TURBULENCE BY THERMALLY AND DYNAMICALLY COUPLED INERTIAL PARTICLES

Hyungwon (John) Park

Dept. of Aero. and Mech. Engineering
University of Notre Dame
Notre Dame, Indiana
Hpark6@nd.edu

Kevin O'Keefe

Dept. of Civil and Env. Eng. and Earth Sci.
University of Notre Dame
Notre Dame, Indiana
Kevin.b.O'Keefe.24@nd.edu

David Richter

Dept. of Civil and Env. Eng. and Earth Sci.
University of Notre Dame
Notre Dame, Indiana
David.Richter.26@nd.edu

ABSTRACT

Direct numerical simulation (DNS) is used to simulate classic Rayleigh-Bénard convection between parallel plates, and Lagrangian point particles two-way coupled in both momentum and temperature are added to investigate their modifications to turbulence and Nusselt number (Nu). The particles experience gravitational settling, and are introduced at the lower wall in such a way that turbulence must overcome settling velocity for the particles to vertically distribute throughout the domain. The particle Stokes number based on the Kolmogorov time scale (St), nondimensionalized settling velocity (V_g/U_{buoy}), mass fraction (ϕ_m), and couplings with the flow are independently and systematically varied so as to determine the dominant effects on turbulent kinetic energy and Nu. We find that for each settling velocity, particles with Stokes number of order unity maximize Nu, corresponding to a peak of clustering and modification of turbulent kinetic energy. Increased mass fractions lead to a linear increase of Nu. It is also shown that particles two-way coupled only through momentum attenuate Nu and enhances turbulent kinetic energy while thermal-only coupling attenuates turbulent kinetic energy and enhances Nu. When both couplings are present, however, thermal coupling overwhelms the attenuation caused by momentum coupling and the net result is an enhancement of Nu.

INTRODUCTION

Many natural and industrial systems involve particulate matter suspended in turbulent flows, and depending on circumstances, the interactions of these particulates may modulate the turbulence compared to an unladen case (Balachandar & Eaton, 2010). For instance, the efficiency at transporting and mixing momentum, heat, and other scalars may be drastically altered due to particle-related phenomena such as preferential accumulation (Squires & Eaton, 1991) or inertially-enhanced settling (Aliseda *et al.*, 2002; Wang & Maxey, 1993). This behavior is based on the small-scale interactions between the individual particles of the dispersed phase and their local surroundings, and depends on particle characteristics such as size, shape, composition, concentration, and initial conditions. Within this context, this study is broadly motivated by natural flows where water droplets are suspended in the the turbulent atmosphere, for example during rain and cloud formation or sea spray ejection near the ocean surface from breaking waves. Understanding the dynamic and thermodynamic feedbacks between droplets and turbulence within these systems is crucial for representing small-scale processes in large-scale weather and climate models (e.g. Shaw (2003)).

Studies on the ability of inertial particles to change turbulence through two-way coupling typically use isotropic turbulence or a type of canonical shear-driven turbulence as their model (e.g., channel flow (Zhao *et al.*, 2013), Couette flow (Richter & Sullivan, 2013*a*), homogeneous turbulent shear flow (Gualtieri *et al.*, 2013), etc.). From these studies, much insights have been discovered regarding the role of particles, particularly their effect in modifying turbulence dissipation in isotropic turbulence or modifying near-wall structures and their associated turbulent Reynolds stresses in laden turbulent channel flow.

In these canonical flows, however, the thermal properties of the particles are not coupled in the dynamics of the turbulence, since buoyancy is neglected as a forcing. However in many environmental flows, where buoyancy forces exist resulting from small density changes in the system, thermal coupling of the particles to the turbulence plays an important role. An example of this in the atmosphere is during cumulus cloud formation, where buoyancy-driven turbulent updrafts are coupled to the formation of water droplets through condensation.

While several studies have sought to include the thermodynamic coupling of particles, for example (Russo *et al.*, 2014), Nakhaei & Lessani (2017), or Zonta *et al.* (2008) for thermally couple particles in turbulent channel flow, these have not typically included particle-induced turbulence modifications via buoyancy. They instead focus on modifications to turbulence only through momentum coupling, where the role of thermal coupling (i.e. allowing the heat exchange between the particle and surrounding fluid) is primarily investigated as a modifier of heat fluxes and not a modifier of the turbulence itself.

Recently, Frankel *et al.* (2016) reported on the effects of heated particles (via external irradiation) which shed plumes that cause significant reduction in the mean settling velocity when suspended in homogeneous turbulence. Here, the turbulence is modified by both momentum and buoyancy coupling, and the reduced settling velocity is a result of the competition between gravitational settling and particle-induced upward buoyant motions. The simulations used Stokes numbers (St being ratio of the particle acceleration timescale to a characteristic flow timescale) of order unity to examine the effects of the accumulation of particles. This work was then extended

by Zamansky *et al.* (2016), who examined the same coupled system of externally heated particles that induced the turbulence. Zamansky *et al.* (2016) observed 2 regimes of significance for St: for small St, the dynamics of the flow are unchanged, and for intermediate St, particles transition to a cluster-based regime where the flow begins to have dependence on St.

Finally, the work of Oresta & Prosperetti (2013) used the classic Rayleigh-Bénard configuration to understand the effect of isothermal particles on the cross-domain heat transfer, as characterized by the nondimensional Nusselt number Nu. The boundary conditions were such that particles settle through the domain due to gravity, and are re-inserted at the top after passing through the lower boundary. In this setup, where the particle temperature is prescribed and constant in time, Oresta & Prosperetti (2013) shows that the momentum coupling of the particles plays an increasing role in modifying Nu with increasing particle size, and that this introduces a reverse one-way coupling effect where the fluid is influenced by the particles but the particles are not influenced by the flow. The overall Nu increased as particle diameter were increased.

The current work focuses on further understanding these particle-induced turbulence modifications due to both momentum and thermal coupling in classic Rayleigh-Bénard flow. In particular, we are interested in cases where (1) the particle temperature is not treated as constant, and (2) where the particles are introduced at the lower boundary, and therefore require turbulence to transport them throughout the domain. This is meant to represent conditions where buoyancy-driven turbulence is responsible for the suspension of thermally conducting particles which can modify turbulence either by direct momentum coupling or by thermally-driven modifications to buoyancy. Basic questions that this work addresses include: (1) When particles have high inertia relative to the turbulence, which coupling is dominant in modifying heat fluxes maintained by the turbulence? (2) What is the significance of the Stokes number, and when order unity do these indicate different coupling regimes in the flow? (3) What is the difference between particle inertia and particle settling velocity in their relevance to modulate the turbulence, and under what situations does one dominate over the other?

METHOD

To explore these main questions, we take the Rayleigh-Bénard convection configuration as our flow simulation. We incorporate the Lagrangian point-particle approximation method with DNS, then enforce both thermal and momentum two-way coupling. The domain is periodic in the horizontal directions, making the plates infinitely parallel to each other and separated by some distance H. The temperature of both plates is held fixed and a no-slip condition is enforced. The DNS code is further explained by Richter & Sullivan (2013*b*), so only brief details are provided here. It uses a pseudo-spectral spatial discretization in both horizontal directions and second-order finite differences in the wall-normal direction. Time integration is done using a third order Runge-Kutta scheme for both carrier and dispersed phases.

An incompressible flow solver is used to solve the carrier phase conservation equations for velocity, pressure, and temperature:

$$\frac{\partial u_i}{\partial x_i} = 0, \tag{1}$$

$$\frac{\partial u_i}{\partial t} + u_j \frac{\partial u_i}{\partial x_j} = -\frac{1}{\rho_f}\frac{\partial p}{\partial x_i} + \nu_f \frac{\partial^2 u_i}{\partial x_j^2} - \beta(T - T_c) g \delta_{3i} + \frac{1}{\rho_f} F_i, \tag{2}$$

$$\rho_f C_{p,f} \left(\frac{\partial T}{\partial t} + u_j \frac{\partial T}{\partial x_j}\right) = k \frac{\partial^2 T}{\partial x_j^2} + S, \tag{3}$$

while simultaneously solving the Lagrangian conservation equations as well:

$$\frac{dx_i}{dt} = v_i, \tag{4}$$

$$\frac{dv_i}{dt} = \frac{1}{\tau_p}(u_{f,i} - v_i) + g\delta_{3i}, \tag{5}$$

$$\rho_p C_{p,p} V_p \frac{dT_p}{dt} = h_T A (T_\infty - T_p). \tag{6}$$

In these equations, u_i is the carrier phase velocity; x_i is the particle location; v_i is the particle velocity; and p is the carrier phase pressure, solved by a Poisson equation in order to ensure a divergence-free velocity field for each time step. ρ_f is the density of the fluid; ν_f is the kinematic viscosity of the fluid; k is the thermal conductivity of the fluid; $C_{p,f}$ and $C_{p,p}$ is the constant pressure specific heat for the fluid and particles, respectively; V_p is the volume of a single particle; $u_{f,i}$ is the local fluid velocity interpolated using sixth-order Lagrange polynomials; and $\beta = 1/T_{ref}$ is the thermal expansion coefficient for an ideal gas with reference temperature T_{ref}. τ_p is the particle acceleration timescale based on Stokes flow: $\tau_p = (\rho_p/\rho_f)d_p^2/18\nu_f$, where ρ_p is the particle density and d_p is the particle diameter. The heat transfer coefficient of the particle, h_T, is given by a dimensionless empirical correlation: $Nu_p = 2 + 0.6Re_p^{1/2}Pr^{1/3}$ (Ranz & Marshall, 1952).

Since we assume the particles are at sufficiently low volume fractions that particle-particle collisions can be neglected, two-way coupling between phases is included by projecting each particle's gain/loss of momentum and energy onto the local carrier phase velocity and temperature field, respectively. The momentum is represented by the F_i term in equation 2 whereas the thermal coupling is represented by the S term in equation 3. These terms are computed by projecting the negative of the individual particle contribution onto the surrounding computational nodes for every individual particle.

The particle's velocity and temperature is not necessarily equal to the surrounding field, as their difference is determined by the droplet momentum and thermal inertia. Each droplet temperature is integrated according to energy conservation and assumes only convective heat exchange with the surroundings based on the droplet and surrounding temperature difference. The heat conduction inside the particles is much faster than the external convection, and therefore we assume the droplet has a uniform interior temperature. The momentum conservation is calculated in the exact same way as the energy equation. We assume material properties for spherical water droplets in air, and since their density ratio, respectively, is O(1000), gravity and hydrodynamic drag are the only relevant forces considered in their governing equation. The Boussinesq approximation is made for the buoyancy forcing in the vertical momentum equation of the carrier phase.

At the top boundary, particles experience perfectly elastic collisions to represent a no-flux condition. When a particle crosses the lower boundary, we remove the particle and re-inject at an-

other location in order to keep the total number of particles constant throughout the simulation. We note that the turbulence of the fluid near the lower surface may be too weak to re-suspend the water droplets, so rather than place the new particles at the top boundary, we position them randomly inside the lower 10% of the domain. Our experience indicates that at approximately 10% of the domain height, the turbulent heat flux and diffusive heat flux are at equal strengths, and thus this is a sufficient height at which turbulence can re-suspend the newly created particles. The velocity and temperature of the particles at re-injection are kept equal to the particle which they are replacing such that the total energy and momentum of our system is conserved (i.e. there are no external sources of energy or momentum).

The field is first spun-up, meaning that the Rayleigh-Bénard configuration is allowed to reach a statistically steady state without any particles. Afterwards, particles are randomly distributed throughout the entire domain into the turbulent field, and averages are computed after a statistically steady state is established.

Finally, the code has been validated against the work of Oresta & Prosperetti (2013). We configured both unladen and laden cases to match as closely as possible their numerical setup (including forcing our particles to be isothermal instead of dynamically varying), and we achieved consistent results.

NUMERICAL EXPERIMENTS

In the simulations, we specifically focus on the role of particle inertia, settling velocity, coupling, and mass fraction. Therefore, each parameter is varied while holding the others constant in order to isolate their individual contributions to the overall influence on heat flux. For all cases, the Rayleigh number is set to $Ra = 2 \times 10^6$ ($Ra = g\beta\Delta T H^3/\nu_f\alpha$, where g is the acceleration due to gravity, ΔT is the temperature difference between the top and bottom walls, and α is the fluid thermal diffusivity). For the settling velocity, we vary the dimensionless quantity V_g/U_{buoy}, where $V_g = \tau_p g$ is the droplet terminal velocity and $U_{buoy} = \sqrt{(g\beta\Delta TH)}$ is a characteristic buoyancy velocity scale. The terminal velocity ratio is varied over the range from $0.0001 \leq V_g/U_{buoy} \leq 0.01$. For understanding the effects of particle inertia, we vary the dimensionless Stokes number based on the buoyancy scale ($St_f = \tau_p/(H/U_{buoy})$), where the range from $0.025 \leq St_f \leq 2.5$ corresponds to St based on the Kolmogorov time scale over a range from $O(0.1) \leq St \leq O(10)$. We intentionally include $St \approx 1$ in our range since this is associated with a peak in particle clustering (Squires & Eaton, 1991; Rouson & Eaton, 2001). St of the system will change based on the momentum coupling because of the particles' potential to change the dissipative scales, altering the Kolmogorov timescale. Lastly, mass fraction, defined as $\phi_m = Nm_p/m_f$ where N is the number of particles in the system, m_p is the mass of an individual particle, and m_f is the mass of the fluid, is varied for specific cases over the range $0.01 \leq \phi_m \leq 0.25$.

Our nondimensional dependent variable is the Nusselt number, the normalized heat flux across the domain. It is defined as $Nu = \overline{q}H/k\Delta T$, where $\overline{q}$ is the vertically averaged total heat flux across the channel, which is the combination of diffusive, turbulent, and particle-induced fluxes of heat. Finally, we vary the couplings between the particles and surrounding flow so that both thermal and momentum, as well as each alone, are simulated for key values of St and V_g/U_{buoy}. For these cases of interest, we want to determine the comparative magnitudes of thermal to dynamic coupling on buoyancy-driven turbulence. Properties of fluid and particles are shown in Table 1. These are constants used in all simulations.

Table 1. Constant fluid and particle properties

Parameter	Value
Cell height, H	0.116 m
Cell width, W	0.348 m
Rayleigh number, Ra	2×10^6
Fluid density, ρ_f	$1.29\,(kg/m^3)$
Kinematic viscosity, ν	$1.37 \times 10^{-5}\,(m^2/s)$
Thermal diffusivity, α	$2.02 \times 10^{-5}\,(m^2/s)$
Temperature difference, ΔT	$10\,(^\circ C)$
Specific heat of particles, $C_{p,p}$	$4.179\,(\frac{kJ}{kgK})$
Specific heat of fluid, $C_{p,f}$	$1.0\,(\frac{kJ}{kgK})$
Buoyancy velocity scale, U_{buoy}	$2.04 \times 10^{-1}\,(m/s)$

RESULTS

Our first simulation was to run an unladen field, get statistically steady-state averages, and use them as a comparison as well as an initial condition for all future simulations.

To illustrate the DNS with the Lagrangian point-particle approximation described in previous Sections, Figure 1 provides a snapshot of the Eulerian field laden with particles. This particular case is for $St \approx 1$ and has temperature contours of the fluid to provide a general representation for how the fluid flows within the enclosed region. Since $St \approx 1$, the particles experience pronounced preferential concentration, accumulating toward the buoyant plumes.

As a contrast, shown in Figure 2 for particles with smaller St; the particles travel much more closely with the fluid motion and therefore do not experience the same degree of preferential accumulation. Similarly, for large St, particles would feel little effects of the fluid flow, possessing too much inertia to be significantly affected, particularly in the regions of buoyant updrafts and downdrafts. In this case, again particles would tend to remain uniformly distributed throughout the field. Figure 2 contains many more particles than Figure 1 in order to maintain the same mass fraction $\phi_m = 0.05$.

The first set of simulations consisted of varying St_f and V_g/U_{buoy} with both couplings present at a constant mass fraction, then comparing the measured Nu against the unladen base case. These results are presented in Figure 3. For all cases considered, the entire range of St and V_g/U_{buoy} enhances Nu compared to the unladen case. Regardless of V_g/U_{buoy}, Nu always increases as St approaches $O(1)$, as preferential concentration is most pronounced in that region. This is why for deviations from $St \approx 1$ Nu is decreasing: the effect of preferential concentration is weakening. When considering the particle settling velocity, the maximum values of Nu exist for $V_g/U_{buoy} = 0.001$ for all St. This effect is less pronounced as St deviates from $O(1)$.

From this information, we focused on $V_g/U_{buoy} = 0.001$, which exhibits the highest Nu, and ran momentum-only and thermal-only couplings over the same range of St in order to elucidate which coupling mechanism is the dominant factor controlling Nu. When divided into different couplings, both of them show unique differences in how they change heat transfer, as shown in Figure 4. In all cases the thermal coupling enhances Nu compared to the unladen case and is at its maximum for $St \approx 1$, and decreases toward the unladen value as St deviates from O(1). For the momentum-

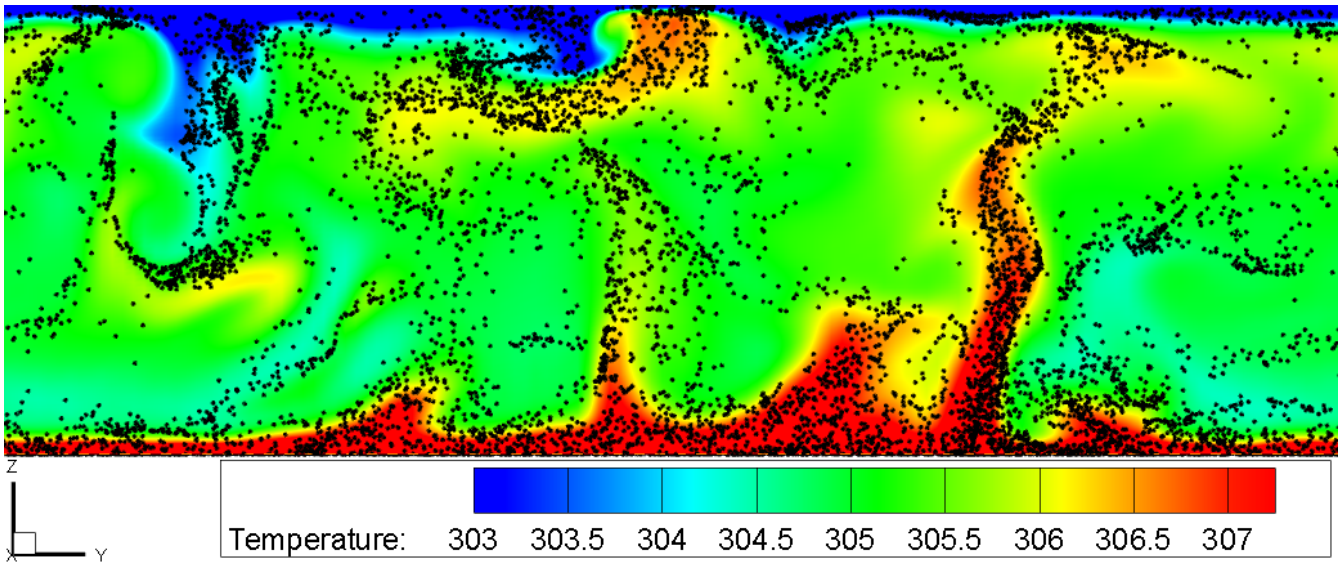

Figure 1. This snapshot is a general representation of the simulations containing particles. This particular one has properties of $St \approx 1$ and $V_g/U_{buoy} = 0.001$, which is evaluated to have the highest Nu. The effect of preferential concentration in the turbulent updrafts and downdrafts are shown here.

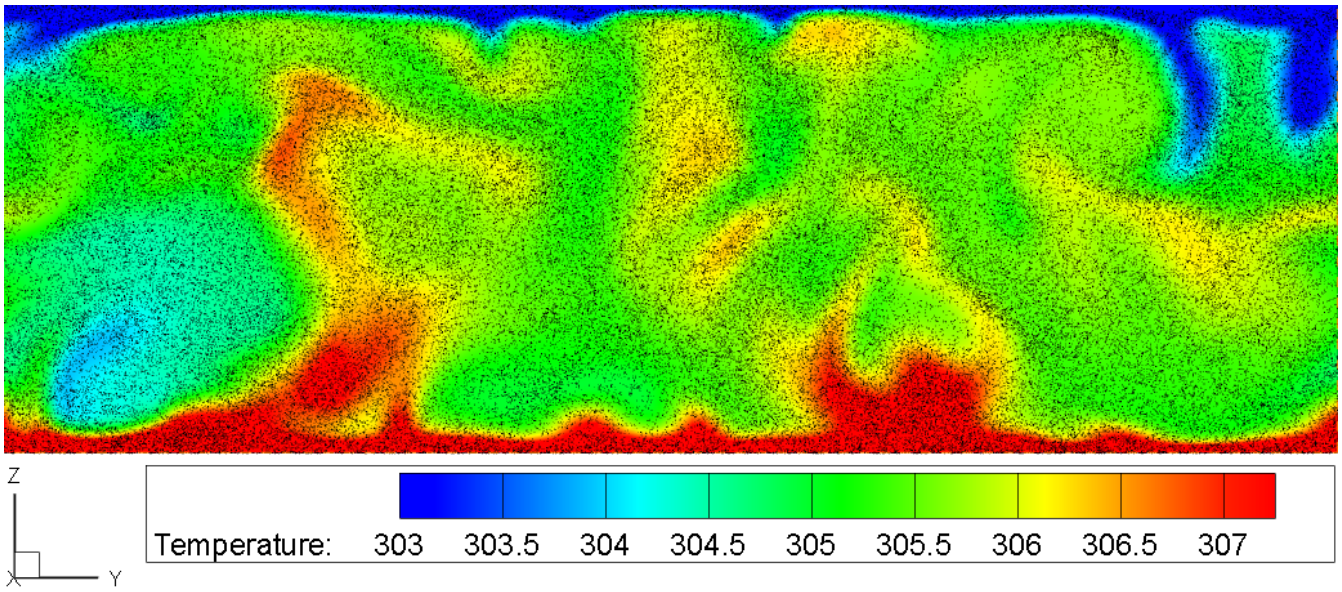

Figure 2. This snapshot is for $St \approx 10$ and $V_g/U_{buoy} = 0.001$. The effect of preferential concentration in the turbulent updrafts and downdrafts is less pronounced.

only cases, all St decreases Nu with respect to the unladen case, while $St \approx 0$ returns to the unladen-based Nu and reaches the lowest decrease of Nu at $St \approx 2$ and remains there for all increasing St. For $St > 1$, the two-way coupling mechanism becomes a net balance between the attenuation of the momentum-coupling and the enhancement of the thermal-coupling, while both-coupling for $St < 1$ is nearly identical to thermal-only coupling.

To partially explain why Nu changes with these different two-way couplings, we look to Figure 5, which is a representative example of the various terms in the total heat flux balance for $St \approx 1$ and V_t/U_{buoy}. The total heat flux is constant in the vertical direction, as expected for this setup. The diffusive heat flux is at its maximum toward the vertical boundaries whereas it is comparatively minimal to the turbulent heat flux toward the center of the domain. The turbulent flux goes to zero at both boundaries. The diffusive flux profile does not vary with different couplings. Displayed in Figure 6, only the profiles of the turbulent heat flux and the particle source heat flux are shown for the different coupling combinations, including the unladen case. An important note of the profiles is that for the momentum-only coupling and unladen cases there exists no particle source heat flux by definition. While the turbulent heat flux is reduced for both and thermal coupling only with particles, the particle source heat flux significantly increases the overall heat flux of the system, increasing Nu. For momentum-only cases, the turbulent heat flux is decreased compared to an unladen simulation, without any thermal particle contribution, and therefore has a decrease in Nu.

Considering Equation 3, Nu is enhanced for both and thermal coupling due to the particles' direct contribution to the convective heat transfer that induces an increased heat flux between fluids at

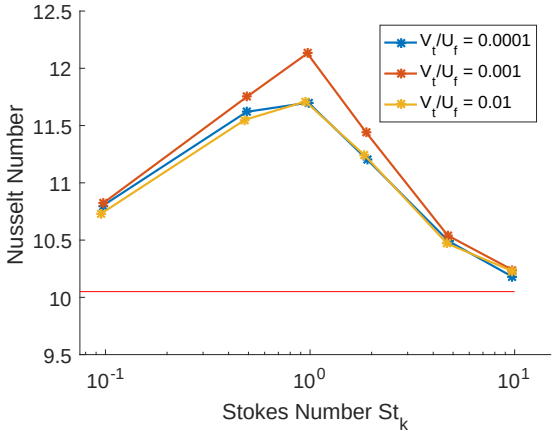

Figure 3. Nusselt numbers as a function of different Stokes numbers and terminal velocity ratio for $\phi_m = 0.05$, with all couplings. The horizontal line is the reference Nusselt Number that corresponds to an unladen field.

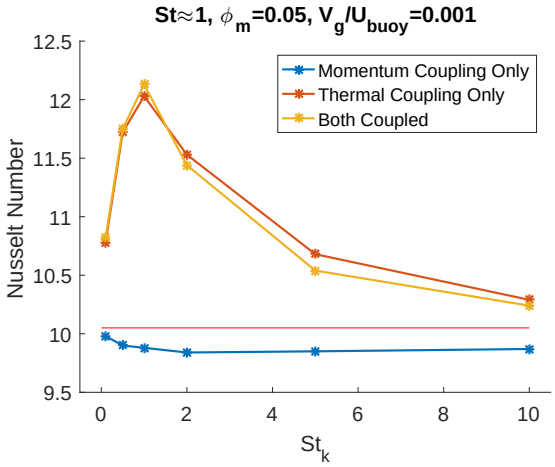

Figure 4. *Nu* based on different couplings. The reference line is the unladen field Nu.

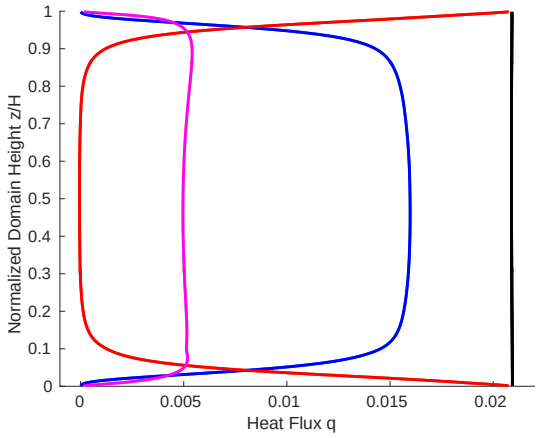

Figure 5. Representative vertical heat flux profiles for the highest *Nu*: $St \approx 1$ with $V_g/U_{buoy} = 0.001$. The different colored lines represent: the turbulent heat flux (blue), the diffusive heat flux (red), the particle temperature source term (purple), and the total vertical heat flux (black). The field contains the same particle parameters as Figure 1.

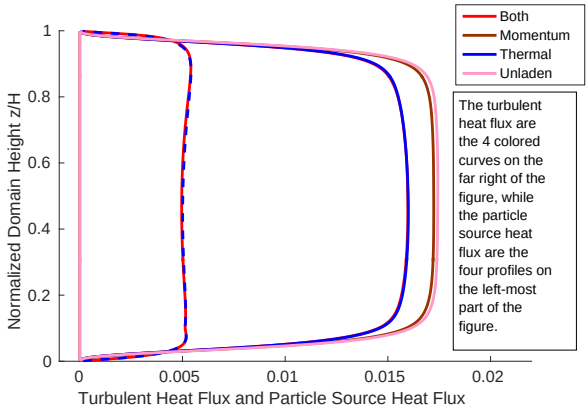

Figure 6. Turbulent and particle contributions to the total heat flux for varying couplings for $St \approx 1$.

different temperatures. As a result the turbulence of the system is weakened as the buoyancy effect in Equation 2 is decreased. This is the balance between the particle source contribution to the heat flux and the decrease in turbulent heat flux that is a consequence of the particles. This can be further understood by considering Figure 7. The both coupling as well as the thermal-coupling profiles have a lower turbulent kinetic energy (TKE) compared to the momentum and unladen cases. This however, is compensated in terms of *Nu* by the particle source heat flux. Also, the effects of the momentum-only coupling is shown to decrease the TKE of the carrier phase, without any contribution to *Nu* by the particle source heat flux.

Finally, we again choose *St* which exhibits the highest *Nu*, which is $St \approx 1$ with $V_g/U_{buoy} = 0.001$, to better understand the effects of changing ϕ_m. An important restriction in the range of ϕ_m is that it must remain in an acceptable range to still be only considering a two-way coupling mechanism (Balachandar & Eaton, 2010). With this mind, the range of the mass fraction was limited to $0.01 \leq \phi_m \leq 0.25$. Figure 8 shows a proportional relationship between *Nu* and ϕ_m for both couplings and thermal-coupling, while momentum-coupling still decreases *Nu*. As the mass fraction approaches 0 the effect of particles revert back to an unladen case. The proportional relationship represents the different mechanisms that change *Nu* for $\phi_m = 0.05$ are not changed with increasing mass fraction.

CONCLUSIONS

From the simulations considered, the particle Stokes number determines much of the interactions between the particles and the flow in terms of the Nusselt number. For intermediate *St*, inertial particles under two-way coupling always enhance *Nu* compared to an unladen field, with the highest *Nu* near $St \approx 1$. *Nu* decreases as *St* departs from $O(1)$ due to the weakening effect of preferential concentration. In terms of the particle settling velocity, there exists a terminal velocity ratio such that the fluid can exhibit a maximum *Nu*, which in our simulations is found to be $V_g/U_{buoy} = 0.001$, again having the most pronounced *Nu* for $St \approx 1$ and decreasing in enhancement as *St* increases or decreases from $O(1)$. With setting $V_g/U_{buoy} = 0.001$, the comparison between couplings shows that the thermal coupling is the dominant enhancement effect of *Nu* as compared to momentum coupling, which decreases *Nu*. The full two-way coupling, however, shows that the thermal coupling is the main enhancer of *Nu* and has little reduction from the momentum

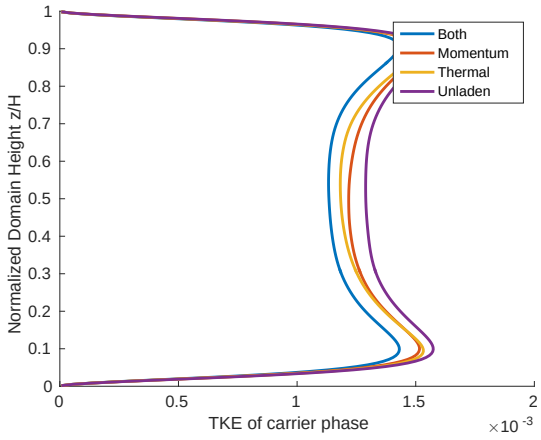

Figure 7. Vertical profiles of the horizontally averaged turbulent kinetic energy for $St \approx 1$ and $V_g/U_{buoy} = 0.001$.

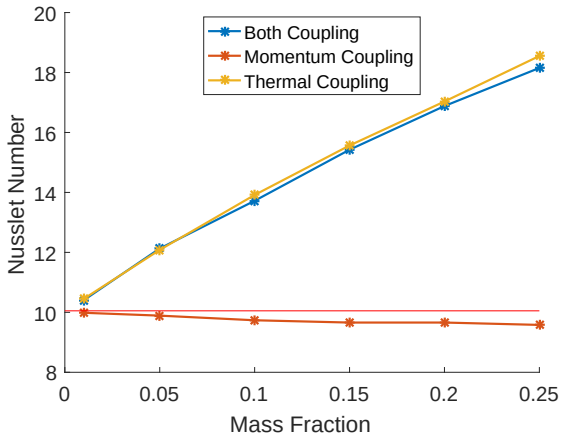

Figure 8. Two-way coupling combinations over a range of mass fractions based on $St = 1$ and $V_g/U_{buoy} = 0.001$.

coupling. The importance behind the coupled effects is that the potential particle source heat flux is balanced from the decrease in buoyancy as a consequence of the enhanced heat flux, as shown by compared TKE and heat flux profiles. Nu is proportional to the mass fraction when both couplings are present, while it has no significant effect in momentum-only coupling. By being proportional to Nu, the mass fraction simply determines the amount of interaction between the fluid and particles, without difference in physical effects for different ϕ_m.

ACKNOWLEDGEMENT

This work was partially supported by the National Science Foundation (NSF) under Grant No. AGS-1429921. Computational resources were provided by the Notre Dame Center for Research Computing.

REFERENCES

Aliseda, A., Cartellier, A., Hainaux, F. & Lasheras, J.C. 2002 Effect of nonlinear drag on the settling velocity of particles in homogeneous isotropic turbulence. *Journal of Fluid Mechanics* **468**, 77–105.

Balachandar, S. & Eaton, John K. 2010 Turbulent Dispersed Multiphase Flow. *Annual Review of Fluid Mechanics* **42** (1), 111–133.

Frankel, Ari, Pouransari, H, Coletti, F & Mani, A 2016 Settling of heated particles in homogeneous turbulence. *Journal of Fluid Mechanics* **792**, 869–893.

Gualtieri, P., Picano, F., Sardina, G. & Casciola, C. M. 2013 Clustering and turbulence modulation in particle-laden shear flows. *Journal of Fluid Mechanics* **715**, 134–162.

Nakhaei, M.H. & Lessani, B. 2017 Effects of solid inertial particles on the velocity and temperature statistics of wall bounded turbulent flow. *International Journal of Heat and Mass Transfer* **106**, 1014–1024.

Oresta, Paolo & Prosperetti, Andrea 2013 Effects of particle settling on Rayleigh-Bénard convection. *Physical Review E* **87** (6), 1–11.

Ranz, W. E. & Marshall, W. R. 1952 Evaporation from drops - Part 1. *Chemical Engineering Progress* **48**, 141 – 148.

Richter, David H. & Sullivan, Peter P. 2013*a* Momentum transfer in a turbulent, particle-laden Couette flow. *Physics of Fluids* **25**, 053304.

Richter, David H. & Sullivan, Peter P. 2013*b* Momentum transfer in a turbulent, particle-laden Couette flow. *Physics of Fluids* **25** (5).

Rouson, Damian W. I. & Eaton, John K. 2001 On the preferential concentration of solid particles in turbulent channel flow. *Journal of Fluid Mechanics* **428** (2001), 149–169.

Russo, E., Kuerten, J. G. M., van der Geld, C. W. M. & Geurts, B. J. 2014 Water droplet condensation and evaporation in turbulent channel flow. *Journal of Fluid Mechanics* **749**, 666–700.

Shaw, Raymond A. 2003 Particle-turbulence interactions in atmospheric clouds. *Annual Review of Fluid Mechanics* **35**, 183–227.

Squires, Kyle D. & Eaton, John K. 1991 Measurements of particle dispersion obtained from direct numerical simulations of isotropic turbulence. *Journal of Fluid Mechanics* **226**, 1–35.

Wang, L.-P. & Maxey, M. R. 1993 Settling velocity and concentration distribution of heavy particles in homogeneous isotropic turbulence. *Journal of Fluid Mechanics* **256**, 27–68.

Zamansky, R, Coletti, F, Massot, M & Mani, A 2016 Turbulent thermal convection driven by heated inertial particles. *Journal of Fluid Mechanics* pp. 390–437.

Zhao, Lihao, Andersson, Helge I. & Gillissen, Jurriaan J. J. 2013 Interphasial energy transfer and particle dissipation in particle-laden wall turbulence. *Journal of Fluid Mechanics* **715**, 32–59.

Zonta, Francesco, Marchioli, Cristian & Soldati, Alfredo 2008 Direct numerical simulation of turbulent heat transfer modulation in micro-dispersed channel flow. *Acta Mechanica* **195**, 305–326.